Influence of the Embedded Length on the Overall Stability of Single Anchored Retaining Walls

C.M. Santos Josefino, N.M.C. Guerra, A.N. Antão

Abstract. Urban excavations are frequently performed using anchored retaining walls. Overall stability is an important stability verification in such walls and is significantly influenced by geometrical and mechanical characteristics of the wall, of the anchors and of the soil. In the present work, particular emphasis is given to the role of the embedded length in reducing the needed anchor length to ensure the overall stability, for the case of single anchored retaining walls. The need to reduce the anchor length can be justified by economical and technical reasons. The problem is analysed using classic limit equilibrium methods and finite element calculations.

Keywords: overall stability, anchored retaining walls, urban excavations, embedded length.

1. Introduction

Overall stability is an important verification for the design of anchored retaining walls. The overall stability of anchored retaining walls depends on the anchor length and on other geometrical parameters such as anchor head depth, anchor inclination and the embedded length of the wall. In this work the influence of these parameters on the minimum anchor length needed to ensure overall stability is studied through a parametric analysis and by using Broms' (1968) classical limit equilibrium method for checking the overall stability of single anchored retaining walls.

The classical methods for overall stability are based on Kranz's (1953) method. This method was initially presented for single anchored retaining walls using plate or beam anchors. It was later extended by Jelinek & Ostermayer (1967) to walls with two or more horizontal plate or beam anchor levels and by Ranke & Ostermayer (1968) to cases involving two or more inclined grouted pre-stressed anchors. Broms (1968) presented an alternative method to Kranz's approach and applied it to single-anchored (grouted, pre-stressed and inclined) retaining walls. These methods are often cited in reference works, such as Hanna (1982), Matos Fernandes (1990) and Puller (1996), explaining how they can be used to check the overall stability, but systematic works showing the practical results on anchor length of the application of such methods could not be found in the literature. Recently, Santos Josefino *et al.* (2014) performed a parametric analysis of Broms' and Kranz's methods showing the influence of different approaches for safety verification on the needed anchor length of single-anchored retaining walls. Conclusions on the required location of the grouted anchor bond were presented. This approach was extended to retaining walls with two anchor levels by Guerra *et al.* (2016).

In the present paper this line of work is proceeded and particular attention is given to the role of the embedded length of single anchored retaining walls as a way of reducing the anchor length needed to ensure the overall equilibrium. The interest of such solution is justified by possible reasons of cost (for cases where the cost of increasing the embedded length of the wall could be compensated by the benefit of decreasing the anchor lengths) but also, most particularly, by geometrical difficulties in using long anchors due to possible proximity to the excavation of buried and/or sensitive structures, in an urban environment. For the analysis of this parameter a series of finite element calculations is performed, their results being presented and compared with the limit equilibrium approach.

2. Classical Limit Equilibrium Methods for the Analysis of Overall Stability

Kranz's (1953) and Broms' (1968) methods are two classical limit equilibrium methods for the analysis of overall stability (Fig. 1). As described by Guerra *et al.* (2016), there are three differences between the two methods: 1) location of point C; 2) definition of safety factor and 3) volume involved in the equilibrium.

Kranz's method and the ones directly derived from it, consider point *C* at the middle of the bond length. Broms' method considers the possibility of other locations for this point, but in the present paper point C will be assumed as in Kranz's method, at the center of the bond length. Therefore, the anchor length assumed in the calculations in Broms' method will be L_u, given by:

Cláudia S. Josefino, M.Sc, Ph.D. Student, Departamento de Engenharia Civil, Faculdade de Ciências e Tecnologia, Universidade Nova de Lisboa, Lisboa, Portugal. e-mail: claudiajosefino@hotmail.com.
Nuno M. da Costa Guerra, Ph.D., Associate Professor, UNIC, Departamento de Engenharia Civil, Faculdade de Ciências e Tecnologia, Universidade Nova de Lisboa, Lisboa, Portugal. e-mail: nguerra@fct.unl.pt.
Armando M.S. Nunes Antão, Ph.D., Associate Professor, UNIC, Departamento de Engenharia Civil, Faculdade de Ciências e Tecnologia, Universidade Nova de Lisboa, Lisboa, Portugal. e-mail: amna@fct.unl.pt.
Submitted on November 4, 2016; Final Acceptance on July 5, 2017; Discussion open until December 29, 2017.

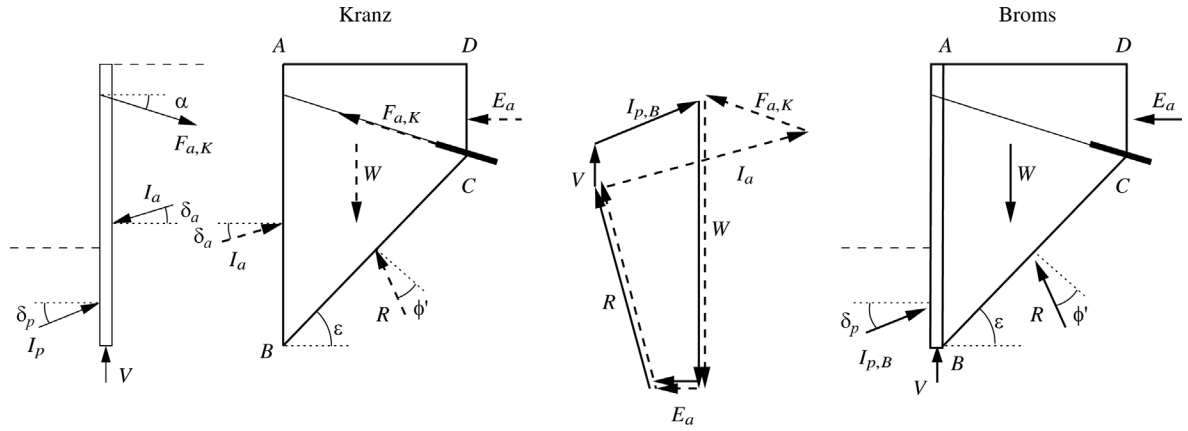

Figure 1 - Geometry of the case study.

$$L_u = L_f + \frac{L_b}{2} \quad (1)$$

where L_f is the free anchor length and L_b is the bond length (Fig. 2).

Safety factors were originally defined in different ways in the two methods. Kranz's method assumes the safety factor, FS_K, to be defined as:

$$FS_K = \frac{F_{a,K}}{F_a} \quad (2)$$

where $F_{a,K}$ is the allowed force on the anchor, determined from Kranz's method, and F_a is the force applied on the anchor. Broms' method considers the safety factor, FS_B, as:

$$FS_B = \frac{I_p}{I_{p,B}} \quad (3)$$

where I_p is the passive force that can be mobilized on the embedded length of the wall and $I_{p,B}$ is the passive force needed to ensure equilibrium, determined from Broms' method.

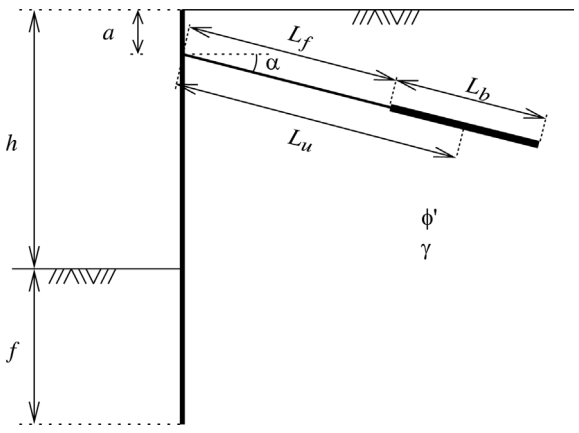

Figure 2 - Kranz's and Broms' methods (adapted from Guerra *et al.* (2016)). Forces for Kranz's method in the polygon are represented by dashed lines; forces for Broms' method are represented by solid lines.

Instead of using those global safety factors, design values of the soil and soil-wall interface properties can be used, and the two methods become equivalent from this perspective also.

Finally, in spite of the differences between these methods concerning the volume involved in equilibrium, they are equivalent. In fact, Broms' method considers the equilibrium of both wall and soil mass ABCD, whereas Kranz's method considers the equilibrium of the soil mass only (Fig. 1). The forces involved in Broms' method (solid lines in the polygon in Fig. 1) are: the passive force, $I_{p,B}$, the vertical force aplied to the toe of the wall, V, the weight of the soil mass *ABCD*, W, the active force, E_a, and the reaction, R. The wall weight was not considered in the present work (and in Fig. 1), but it could easily be included. Also, force V was considered equal to zero. This approch is conservative and the force is probably small in cases of steel sheet-piles or other walls with small cross section. Kranz's method considers equilibrium of the wall and of the soil mass *ABCD* separately. The equilibrium of the wall involves the anchor force, F_a, the active earth pressure, I_a, the passive earth pressure, $I_{p,B}$ and the vertical force aplied to the toe of the wall, V. The forces involved in the equilibrium of the soil mass *ABCD* (the ones involved in Kranz's method, represented by dashed lines in the polygon of Fig. 1) are: the active earth pressure, I_a, the weight of the soil mass, W, the active earth pressure developed along *CD*, E_a, the reaction, R and the anchor force, F_a. If all applied forces are in equilibrium (and, in particular, if the wall is in equilibrium), the two methods will be equivalent.

In the present paper, Brom's method is used.

3. Definition of the Case Study

A case study with the very simple geometry presented in Fig. 2 was considered. The retaining wall has one level of prestressed anchors and is suporting an excavation of depth

h in a homogeneous and dry soil with a friction angle ϕ' and unit weight γ, without surface loads on the supported soil. The anchors make an angle α with the horizontal plane. The embedded length of the wall is f and the depth of the anchor head is a; the soil-to-wall friction angle is δ.

Stability of this kind of structure is ensured by the passive earth pressure developed along the embedded length and by the anchor force. The embedded length and the anchor force were determined using the free-earth support method (Costet & Sanglerat, 1975). Full equilibrium of the wall (including vertical equilibrium) is ensured by using the methodology from Frank *et al.* (2004). This method uses an iterative procedure where full equilibrium is obtained by considering the possibility of the soil-to-wall friction angle not being fully mobilized on either the active side, with friction angle δ_a, or the passive side of the wall, with friction angle δ_p (Fig. 1). In the problem addressed in the present paper, it is the friction angle on the active side that needs adjustment (vertical equilibrium can only be obtained by decreasing δ_a; a decrease in δ_p would further unbalance vertical forces). Active earth pressure coefficients were determined using Coulomb's theory (Coulomb, 1776), through the equation of Müller-Breslau (1906); passive earth pressure coefficients were those from Kérisel & Absi (1990).

Equations of equilibrium of moments and of horizontal forces were used for a first iteration of the anchor force and of the embedded length. The equation of equilibrium of vertical forces was then used to determine the mobilized value of the soil-to-wall friction angle, δ_a, less or equal to δ, which ensured vertical equilibrium. This new value of the soil-to-wall friction angle was then used to perform a second iteration, with updated active earth pressure coefficients, again using equilibrium equations of moments and of horizontal forces. The procedure continued until full equilibrium was achieved for the desired margin of error.

For the simple case presented in Fig. 2, this procedure can be carried out in a dimensionless way, allowing the anchor force and the embedded length to be determined dimensionlessly - $F_a/(\gamma h^2)$ and f_0/h - as a function of ϕ', δ, α and a/h. Symbol f_0 represents the embedded length determined from the free-earth support method. In the present case f is equal to f_0; further in the paper cases where $f > f_0$ will be analysed.

The case study presented considered ϕ' = 30°, $\delta = 20°$, $\alpha = 15°$ and $a/h = 0.2$. Calculations were performed using Design Approach 1 (combination 2) of Eurocode 7 (EN 1997-1, 2004), which uses a partial factor for the friction angles of 1.25, resulting in $\phi'_d = 24.8°$ and $\delta_d = 16.2°$ (d in subscript denotes design values). As in this example there are no variable actions, all other partial factors are equal to 1.0 (EN 1997-1, 2004).

Results of the iterative procedure are presented in Table 1. Final values obtained are $f_0/h = 0.3729 (\approx 0.37)$ and $F_{ad}/\gamma h^2 = 0.1184$.

4. Application of Broms' Method

4.1. Determination of the anchor length needed to ensure overall stability

The vertical equilibrium of the forces involved in Broms' method (Fig. 1) results on the following equation:

$$R = \frac{W - I_{p,B} \sin \delta_p}{\cos(\varepsilon - \phi')} \tag{4}$$

where angle ε (Fig. 1) is given by:

$$\varepsilon = \arctan \frac{h + f - a - L_u \sin \alpha}{L_u \cos \alpha} \tag{5}$$

The horizontal equilibrium results in:

$$I_{p,B} \cos \delta_p - E_a - R \sin(\varepsilon - \phi') = 0 \tag{6}$$

The equations presented above also allow the calculation of the value of L_u required for equilibrium and can be re-written in a dimensionless way (as shown in a different form by Schnabel Foundation Company (1996) and Elton & Whitbeck (1997)). In fact, the ratio L_u/h can be written as a function of other dimensionless parameters:

$$\frac{L_u}{h} = f\left(\phi'; \alpha; \frac{f}{h}; \frac{a}{h}\right) \tag{7}$$

These equations were programmed in Fortran 90 for the geometry of the case study shown in Fig. 2.

4.2. Case study results

The procedure described above was applied to the case presented in section 3 and considering the value of $f_0/h = 0.37$ determined in the same section. The result obtained for dimensionless length L_u/h is 1.245. This length is the minimum length needed to ensure the verification of safety according, again, to Design Approach 1, combination 2 of Eurocode 7. Figure 3 shows the mecanism involved in this calculation.

In this calculation the only safety factor involved is the one applied to the friction angles (equal to 1.25), and

Table 1 - Results of the iterative procedure for determining the embedded length and anchor force for the case study.

Iteration	δ_{ad} (°)	f_0/h	$F_{ad}/(\gamma h^2)$
1	16.2343	0.34895	0.1060
2	6.2996	0.37394	0.1189
3	6.6983	0.37286	0.1184
4	6.6859	0.37289	0.1184
5	6.6863	0.37289	0.1184

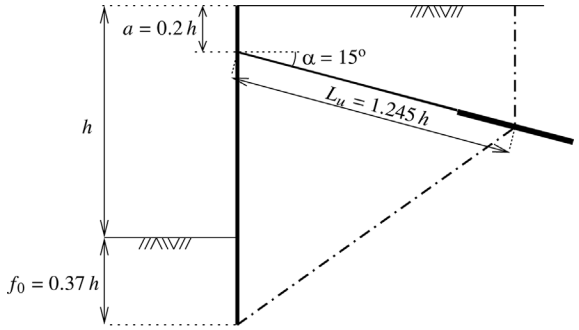

Figure 3 - Broms' mechanism obtained for the case study ($\phi'_d = 24.8°$, $\delta_d = 16.2°$).

therefore this result of the length L_u can be interpreted either as the value that ensures safety for $\phi' = 30°$ or as the value that corresponds to limit equilibrium situation for $\phi' = 24.8°(\approx 25°)$. So, in the following analyses the values of ϕ' can either be the characteristic values of the friction angle (and the results will be the limit equilibrium case) or the design values of the friction angle (and the results will be the minimum to verify safety, in an approach where safety is considered in this way).

4.3. Parametric analysis

4.3.1. Introduction

The main purpose of this paper is to analyse the influence of the embedded length of the wall on the overall stability and, particularly, on the possibility of using shorter ground anchors. However, results also depend significantly on other mechanical and geometrical parameters, such as the soil friction angle, the anchor inclination and the depth of the anchor head. The influence of these parameters will therefore be briefly analysed first. In all cases the soil-to-wall friction angle is assumed equal to 2/3 of the soil friction angle.

4.3.2. Influence of the soil friction angle

To study the influence of the soil friction angle, the previous calculations were repeated for different values of this parameter. Free-earth support method, using the procedure of Frank *et al.* (2004), to evaluate the embedded length and anchor force ratios, and Brom's method, to determine the anchor length ratio L_u/h, were used in the same way. Anchor inclination and depth ratio of anchor head were kept with the previous values of $\alpha = 15°$ and $a/h = 0.2$.

Results for f_0/h, L_u/h and L_u/f_0 are shown in Fig. 4 (in fact, Fig. 4 also presents results for other values of α but only the case of $\alpha = 15°$ is now commented).

Figure 4 shows that, as expected, the embedded length ratio of the wall f_0/h decreases significantly with the soil friction angle, as does the anchor length ratio L_u/h. The anchor ratio decreases less than the embedded length, as demonstrated by the values of L_u/f_0, which show a significant increase with the increase of the soil friction angle. These findings are not surprising. It is well-known that in the equilibrium of this type of retaining walls, the passive force plays an extremely important role, and this role is strongly influenced by the soil friction angle. The role of the friction angle on the overall stability is important, but not as vital as in the case of the wall equilibrium. In fact, the passive force does not play such a crucial part in the overall stability as it does in the wall equilibrium.

4.3.3. Influence of anchor inclination

The influence of anchor inclination was studied repeating previous analyses (performed for $\alpha = 15°$) for other values of angle α - 0, 30 and 45°. Results obtained are also

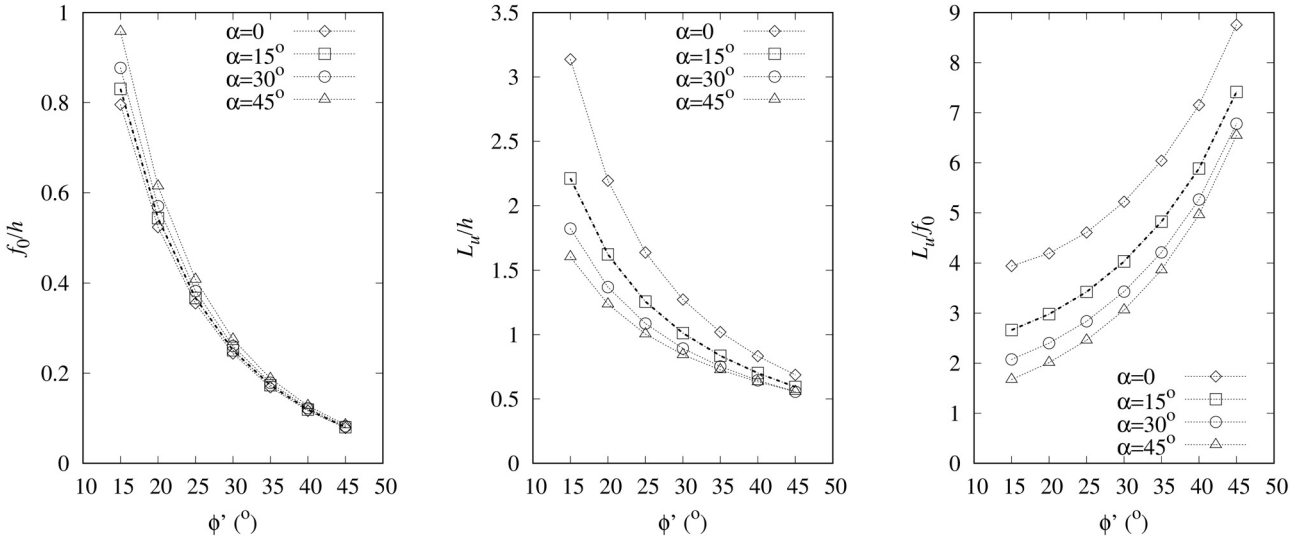

Figure 4 - Values of f_0/h, L_u/h and L_u/f_0 as a function of the soil friction angle for different anchor inclinations and for $a/h = 0.2$ and $\delta/\phi' = 2/3$.

presented in Fig. 4. Anchor inclination has some effect on the embedded length, although relatively small. Greater values of anchor inclination lead to greater embedded lengths, which is needed to ensure vertical equilibrium, as more inclined anchors apply larger vertical forces to the wall. The effect on the anchor length needed to ensure the overall stability is the oposite: greater anchor inclinations lead to shorter anchor lengths, which can be explained by the deeper mechanisms associated to more inclined anchors. Results of L_u/f_0 are therefore greater for less inclined anchors.

4.3.4. Influence of the depth of the anchor head

All previous results were obtained for the depth ratio of the anchor head, *a*/*h*, equal to 0.2. To analyse the influence of this depth, calculations were repeated for other values of *a*/*h* (0.4 and 0.6), for the case of $\alpha = 15°$ and for different soil friction angles. Results are shown in Fig. 5.

The figure shows that both f_0/h and L_u/h ratios decrease with the increase of *a*/*h*. The decrease of f_0/h is a consequence of the equilibrium of the wall, which involves a greater force on the anchor for greater values of *a*/*h*, and the decrease of L_u/h is caused by the deeper mechanisms involved for greater *a*/*h* (for the same anchor inclination) in a way similar to that observed in the previous section. Ratio L_u/f_0 is greater for greater *a*/*h* ratios and assumes the lowest values for the intermediate case of *a*/*h* = 0.4.

4.3.5. Influence of the embedded length

The influence of the embedded length is studied by initially considering the case $\phi' = 30°$, $\alpha = 15°$ and *a*/*h* = 0.2, and repeating calculations using Broms' method for embedded length ratios *f*/*h* greater than f_0/h (or, in another way, considering different f/f_0 ratios). Results are presented by the points marked "$\phi' = 30°$" in the left graphic ($\alpha = 15°$) of Fig. 6; the other lines will be addressed next.

Graphics in Fig. 6 were prepared using the same scale horizontally and vertically. It can therefore be observed that a small increment in *f*/*h* results in a significant decrease in L_u/h. In fact, an increase in *f*/*h* of 0.05 results in a decrease in L_u/h of about 0.30, which shows the effectiveness in the overall stability of increasing the embedded length. Results also show that Broms' method gives no solution for L_u beyond a certain value of *f*/*h*. In fact, the point corresponding to the greatest value of *f*/*h* (and the lowest value of L_u/h) is the last for which Broms' method gives a solution and this corresponds to the situation where the anchor length is still outside the active wedge behind the wall (defined from the wall toe and also marked in Fig. 6). For embedded lengths beyond this case, there is no solution from Broms' method. This does not mean, however, that increasing the embedded length would not further reduce the required value of L_u/h; it only means that the ratio L_u/h can no longer be determined by Broms' method. This will be addressed in the next section.

Results for other friction angles of the soil are also presented in Fig. 6 and similar conclusions may be drawn. The active wedges limit the cases for which solutions from Broms' method can be found in the way previously described. Also, it can be concluded that the reduction in the needed anchor length by increasing the embedded length of the wall is more effective for lower values of the anchor inclination, due to the shallower mechanisms involved, and for lower values of the soil friction angle, due to the more inclined active wedges and therefore the narrower range for which Broms' method gives solution.

A different representation of the same type of results is shown in Fig. 7. The influence of the soil friction angle is

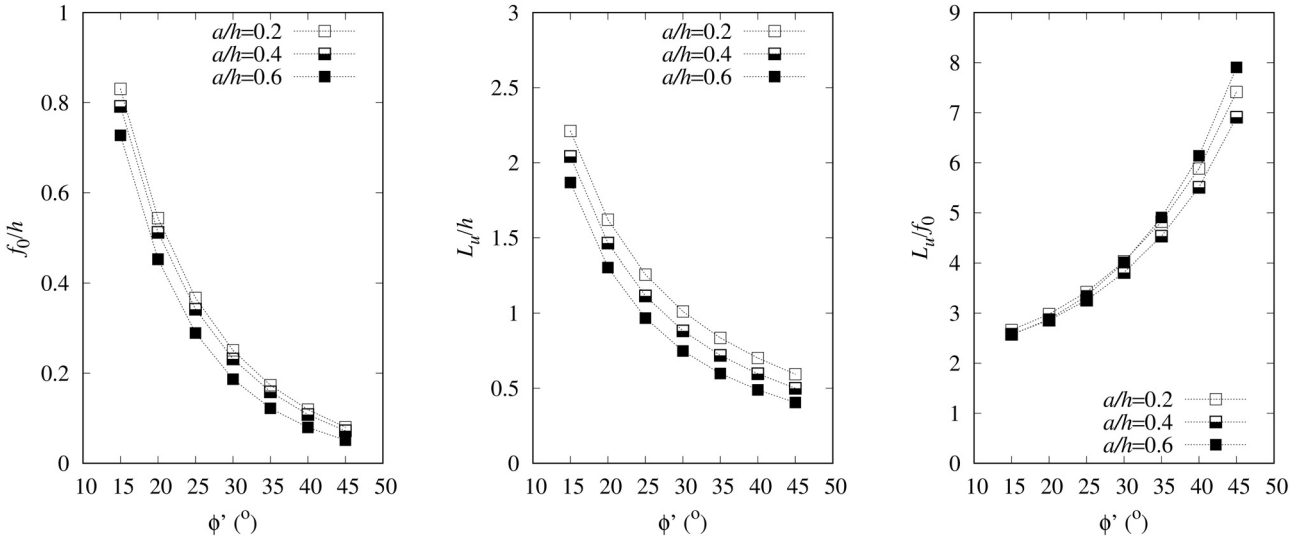

Figure 5 - Values of f_0/h, L_u/h and L_u/f_0 as a function of the soil friction angle for different depth ratios of the anchor head and for $\alpha = 15°$ and $\delta/\phi' = 2/3$.

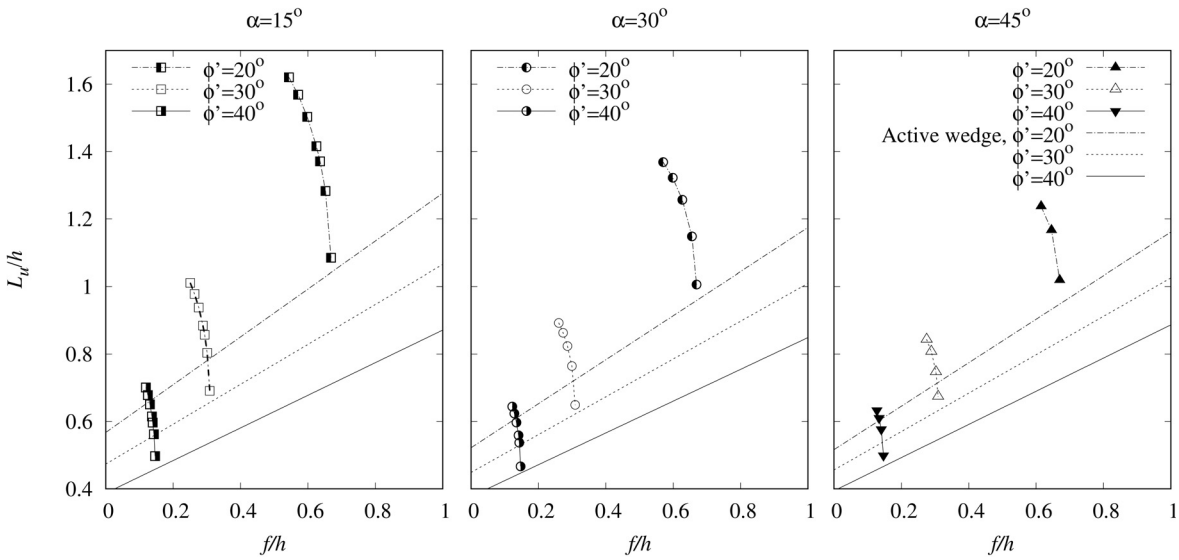

Figure 6 - Values of L_u/h as a function of the embedded length ratio, f/h, for different soil friction angles and anchor inclinations, for a/h = 0.2 and δ/ϕ' = 2/3.

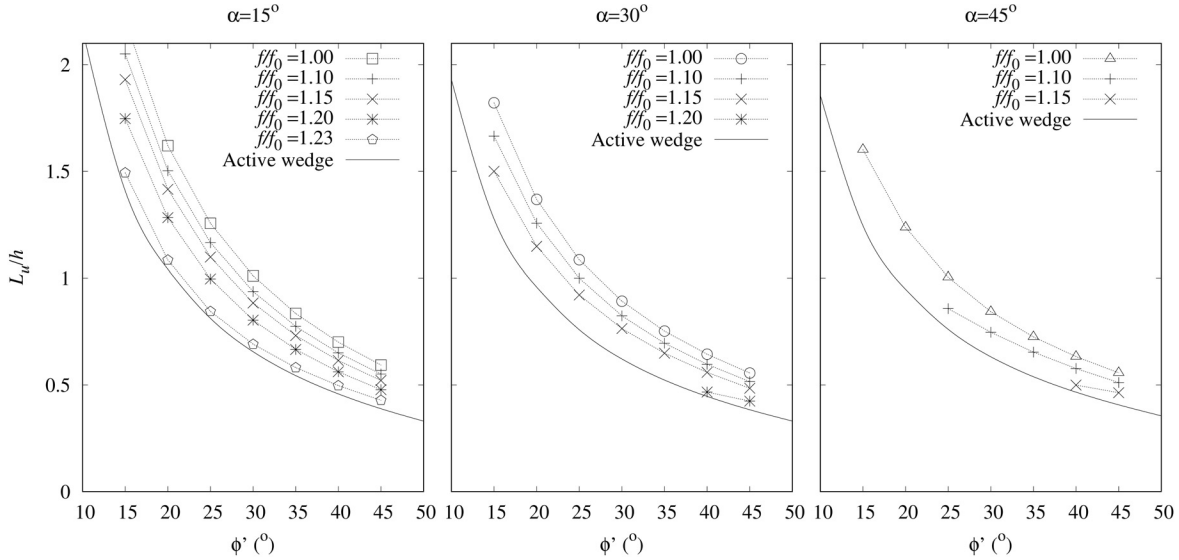

Figure 7 - Values of L_u/h as a function of the soil friction angle, ϕ', for different ratios f/f_0, different anchor inclinations, for a/h = 0.2 and δ/ϕ' = 2/3.

emphasized in this representation, as is the fact that beyond a certain f/f_0 ratio results can not be obtained.

5. Application of the Finite Element Method

5.1. Introduction

Results presented in the previous section highlighted the effectiveness of the increase of the embedded length of single-anchored retaining walls on the needed anchor length to ensure the overall stability. This was shown using a classical method, Broms' method, which had the versatility to provide these conclusions, which seem logical, but also showed some limitations beyond a certain value of the embedded length. Therefore, a finite element approach was also used for comparison with the limit equilibrium results and for further extending the study of the role of the embedded length of the wall on the overall stability of single-anchored retaining walls.

5.2. Description of the case study

The geometry of the case study presented in section 3 was modelled using the finite element program (Plaxis, 2014). A plane strain two-dimensional model was used. A total excavation depth of 10 m was assumed and an embedded length equal to 3.7 m was considered. The anchor head is at 2 m depth and the anchor is inclined at 15°. The anchor

length L_u is 12.45 m; a bond length of 5 m was considered in the calculations and therefore a free length of 9.95 m was used.

The soil was modelled using the Hardening Soil Model (Schanz *et al.*, 1999). This model is based on the hyperbolic relationship between strains and stresses, but is elastoplastic. The yield surface of the model is not fixed in the principal stress space; it can expand due to plastic straining (hardening). The model uses compression hardening to model the evolution of plastic strains due to primary compression, and shear hardening for the plastic strains due to primary deviatoric loading. It uses the theory of plasticity, includes soil dilatancy and a yield cap (Plaxis, 2014).

The model uses three input stiffnesses: the secant triaxial loading stiffness to half of the strength, E_{50}, the triaxial unloading and reloading stifness, E_{ur}, and the oedometer loading stiffness, E_{oed}. These stiffnesses depend on the stress state according to the following equations:

$$E_{50} = E_{50}^{ref}\left(\frac{c'\cos\phi' + \sigma'_3 \sin\phi'}{c'\cos\phi' + p^{ref}\sin\phi'}\right)^m \quad (8)$$

$$E_{ur} = E_{ur}^{ref}\left(\frac{c'\cos\phi' + \sigma'_3 \sin\phi'}{c'\cos\phi' + p^{ref}\sin\phi'}\right)^m \quad (9)$$

$$E_{oed} = E_{oed}^{ref}\left(\frac{c'\cos\phi' + \sigma'_3 \sin\phi'}{c'\cos\phi' + p^{ref}\sin\phi'}\right)^m \quad (10)$$

where ϕ' is the friction angle, c' is the effective cohesion, m is an exponent that expresses the dependence of the soil stiffness on the stress state in the soil, p^{ref} is an isotropic reference stress, usually taken equal to 100 kPa, σ'_1 is the major principal stress and σ'_3 is the minor principal stress. As a default setting, the program considers $E_{ur}^{ref} = 3E_{50}^{ref}$ and $E_{oed} = E_{50}$.

The case study considers an excavation in a homogeneous material, a dry sandy soil. The moist unit weight was set to 20 kN/m^3. A friction angle equal to 30° and a soil dilatancy equal to 0 were adopted. The stiffness parameters adopted intended to model a loose to medium compact sand and were: $E_{50} = E_{oed} = 15000$ kPa and $E_{ur} = 45000$ kPa. Coefficient m was taken equal to 0.5. The at rest earth pressure coefficient, K_0, was considered equal to 0.5.

The wall was modelled using plate elements, considering elastic behavior, with a bending stiffness, EI, of 1 x 10^6 kNm^2/m and a null Poisson's ratio, due to the plane strain assumption. The interface between the wall and the soil was simulated using joint elements, on both sides of the wall. The strength and stiffness properties of these elements are defined by the strength reduction factor, $R_{inter} = \tan\delta/\tan\phi'$ (Plaxis, 2014), set as 0.63, which corresponds to a δ/ϕ' ratio of 2/3.

The anchor level was modelled by a combination of a node-to-node anchor (free length) and a geogrid (bond length). The material of node-to-node anchor was assumed linear elastic with a stiffness, EA, equal to 56000 kN/m. The bond length was considered linear elastic also, with stiffness equal to 471200 kN/m. The anchor force is equal to 236.8 kN/m (the value determined in section 3).

The calculation consists of an initial stage plus seven construction stages. In stage 0 the initial stresses are generated; in stage 1, the wall is activated (plate and joint elements); in stage 2, the first 3 m of the soil are excavated; in stage 3 the level of anchors is installed and pre-stressed; in the next stages the soil is excavated down to 6 m (stage 4), 8 m (stage 5) and 10 m (final excavation stage). In stage 7 a safety analysis is performed using the c - ϕ reduction feature of the f.e. program, which allows determining the value of ϕ' that causes failure of the soil. The additional displacements that are generated in this stage do not have a physical meaning, but the incremental displacements and the incremental shear strains give an indication of the likely failure mechanism.

5.3. Results

Results obtained in the calculation for the displacements of the wall and of the surface of the supported soil are represented in Fig. 8, for different stages, until the final excavation. Results for the c - ϕ reduction stage are not represented. It can be observed that the initial 3 m excavation causes very small displacements and the effect of pre-stressing the anchor level is clearly seen in the wall displacements and also on the swelling of the soil surface, which is due to the anchor bond and the effect of the anchor force. Subsequent excavation stages cause an increase of the displacements. For the final excavation stage, displacements increase significantly, the horizontal displacements of the wall reaching 0.3% of the total height and the settlements of the surface of the supported soil about half that value.

Figure 9 shows the anchor load changes at each stage. Each excavation stage after anchor activation causes an increase in the anchor load, reaching a maximum of about 18% at the final excavation stage.

In stage 7, after modelling the 10 m excavation, a c - ϕ reduction analysis was performed. The determined value of ϕ' at collapse was 23.85° and the failure mechanism can be inferred from the total displacements presented in Fig. 10. The failure mechanism clearly involves the anchor, showing a typical overall stability mechanism. A passive wedge can be seen in front of the embedded length of the wall.

A comparison with the Brom's mechanism that had been obtained in section 4.2. (Fig. 3) and which is superposed to the one obtained from the numerical calculations shows a relatively good agreement; the main differences are (1) the fact (expected in two-dimensional analysis) that the mechanism from f.e.m. extends to the end of the bond length and does not stop at L_u and (2) the fact that there is a curved shape in the mechanism between the wall toe and

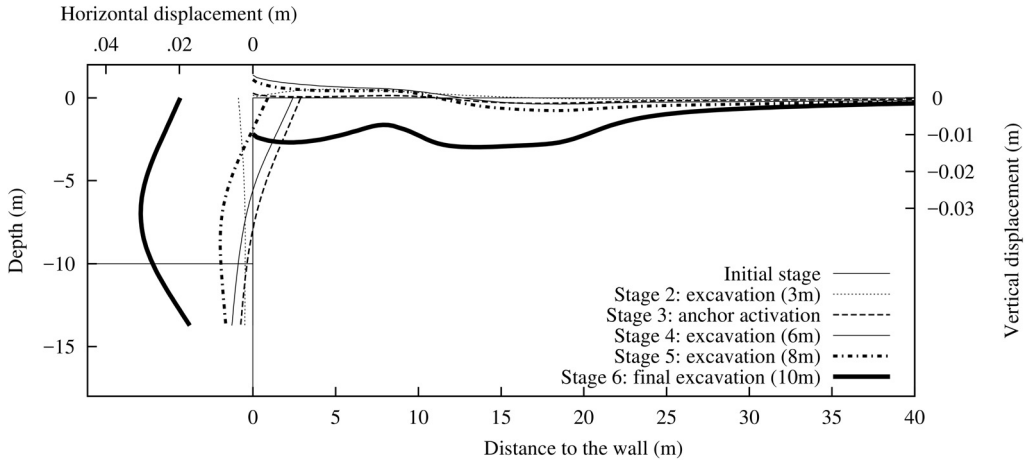

Figure 8 - Horizontal displacements of the wall and settlements of the surface of the supported soil obtained for the numerical case study.

the anchor, which is more realistic (Littlejohn, 1972), whereas Broms' method uses a rectilinear failure surface.

5.4. Parametric analysis

The procedure described in the previous section using the finite element program Plaxis was then repeated for different values of the embedded length ratio, *f*/*h*, and for different anchor length ratios, L_u/h. Four ratios *f*/*h* (0.31, 0.37, 0.43 and 0.55) were tested, for anchor length ratios L_u/h between 0.63 and 2.00. For all calculations the soil friction angle in the collapse was determined using Plaxis' *c* - ϕ reduction feature. The results obtained are shown in Fig. 11, where values obtained from Broms' method are also represented.

It can be seen in Fig. 11 that for constant embedded length, greater soil friction angles lead to the need for shorter anchor lengths. This main conclusion was expected and can be drawn from both the numerical results, represented by the points, and Broms' method, represented by the lines. The lines representing results of Broms' method have two zones: a solid line, for cases where f is greater or

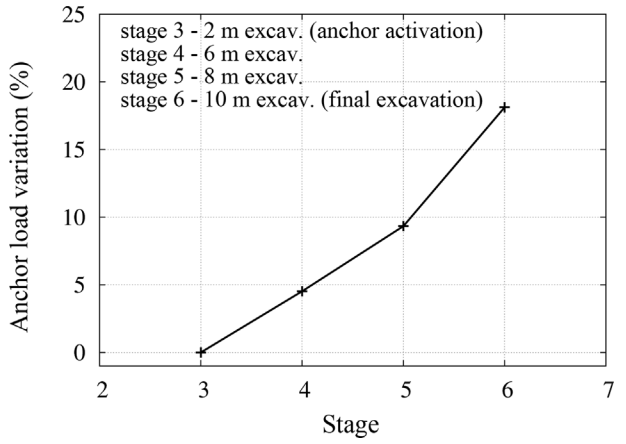

Figure 9 - Anchor load changes obtained for the numerical case study.

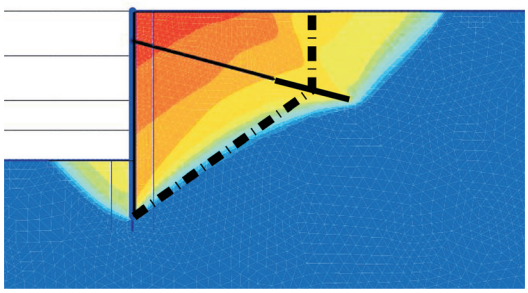

Figure 10 - Failure mechanism inferred from the graphic representation of the total displacements at the *c* - ϕ reduction stage. Comparison with the mechanism using Broms' method.

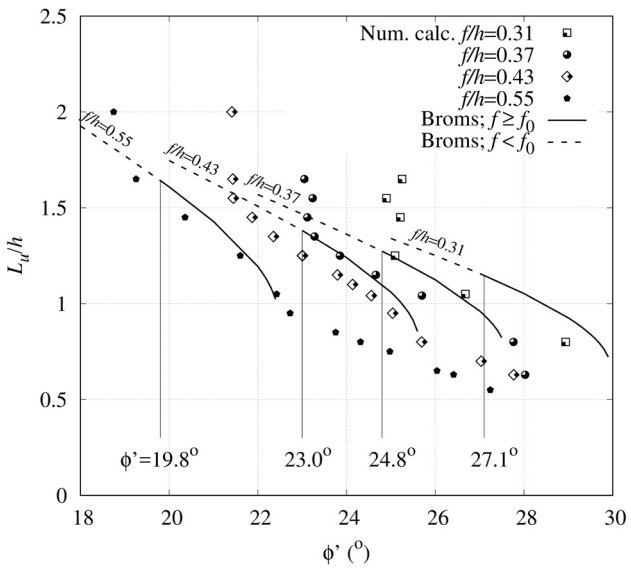

Figure 11 - Limit values of L_u/h as a function of the soil friction angle, ϕ' obtained in the numerical calculations, for different embedded length ratios, *f*/*h*; comparison with the results from Broms' method.

equal to f_0 and a dotted line, for f less than f_0. For example, for $\phi' = 24.8°$, the ratio f_0/h (the one corresponding to the limit case, as seen in section 3), is 0.37 and so this value of the friction angle separates the dotted line from the solid line for this embedded length ratio. Also, the corresponding value of L_u/h is 1.245, as seen in section 4.2. The other values of these limit soil friction angles are indicated in the figure for the other embedded length ratios. If the numerical results were exactly the same as the analytical calculations, there should be no points to the left of these vertical lines, because the equilibrium of the wall would not be possible for friction angles lower than that limit value.

Naturally, finite element calculations do not correspond exactly to the limit equilibrium model and there are points to the left of those vertical lines, as in the case study of the previous section. But it can also be seen that there is a limit of friction angles (lower than the limit value from limit equilibrium) below which there are no results. This can be seen, for example, for $f/h = 0.31$; the limit friction angle from limit equilibrium calculations is 27.1°, but the limit friction angle from the numerical calculations seems to be around 25°. The points, representing the numerical calculations, are thereafter aligned vertically, which means that beyond a certain value of the anchor length L_u/h the friction angle corresponding to failure does not change.

These results can be understood by analysing the mechanisms involved. Some of those mechanisms are represented in Fig. 12. From this figure it can be seen that for a given f/h, up to a certain anchor length ratio L_u/h, the mechanisms can be recognized as typical overall stability mechanisms. It can also be seen that for these overall stability cases, the mechanisms involve a larger volume of soil for longer anchor lengths. These larger volumes of soil correspond, as has been seen from Fig. 11, to lower soil friction angles at collapse, or, as stated, lower soil friction angles need longer anchors to ensure overall stability. But after a certain anchor length, the mechanisms change and seem to become much simpler, with typical active and passive wedges behind and in front of the wall, respectively (in fact in some cases some transitional mechanisms exist between the two - overall and active/passive). These simpler mechanisms correspond to the condition of the stability of the wall and are no longer dependent on anchor length and therefore correspond to the numerical limit of the soil friction angle mentioned before.

Results presented in Fig. 11, although interesting, can not be used directly either to compare or to complete the type of information that was shown in Fig. 6. To do so, part of the results from Fig. 11, for a chosen value of the soil friction angle (for a certain vertical line) must be repre-

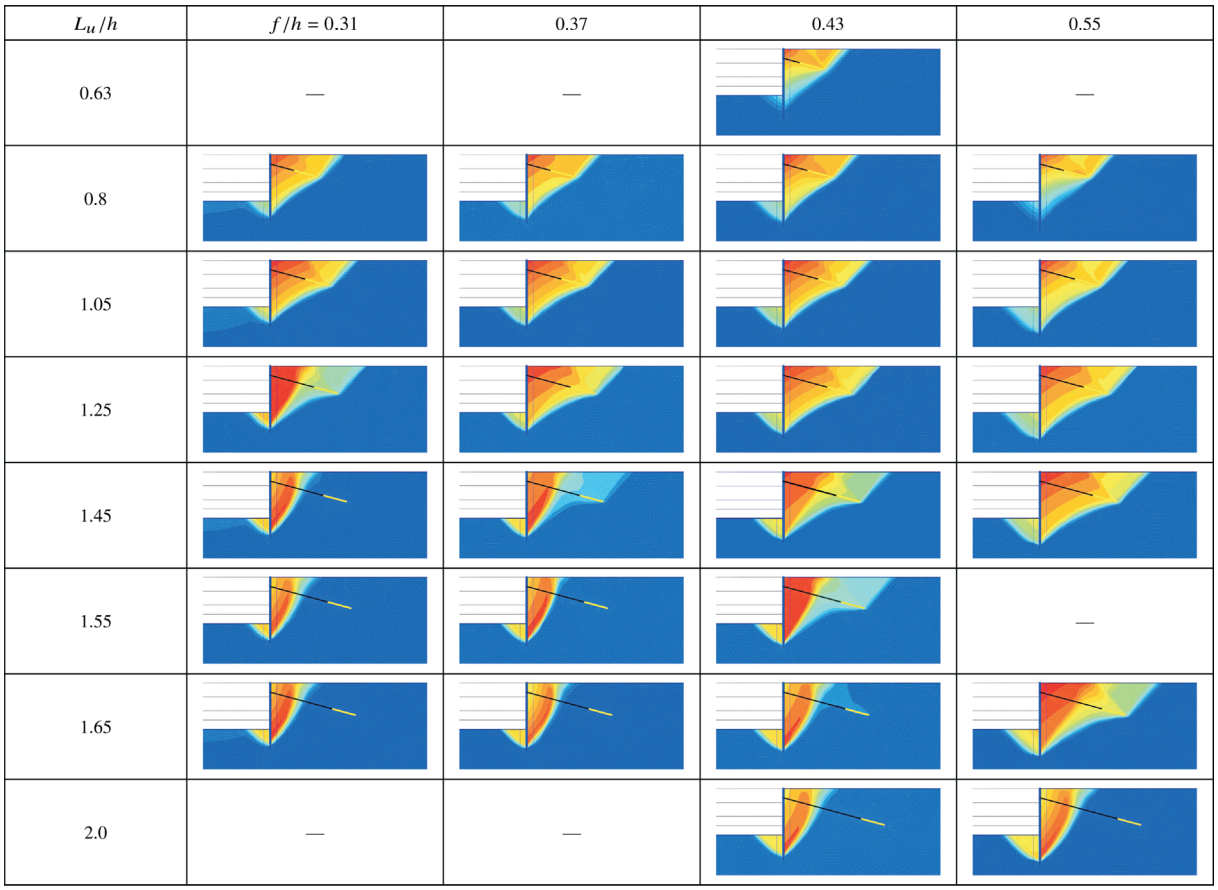

Figure 12 - Mechanisms obtained for most results presented in Fig. 11.

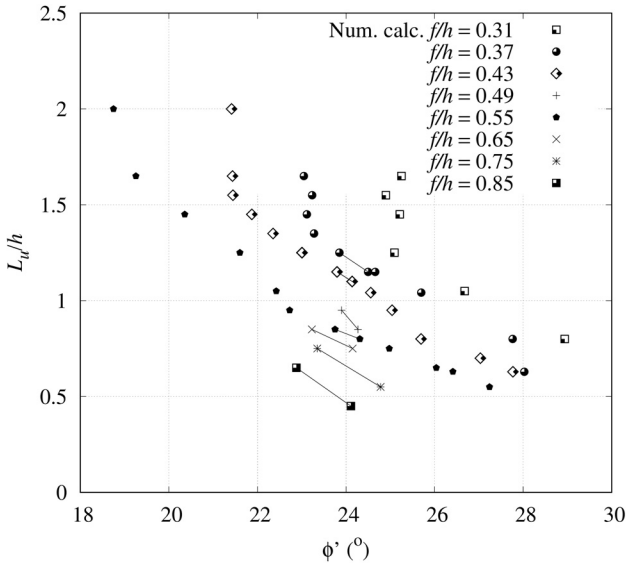

Figure 13 - Limit values of L_u/h as a function of the soil friction angle, ϕ' obtained in the numerical calculations, for different embedded length ratios, f/h; points used for interpolation for determining L_u/h for ϕ' = 24° are linked by a solid line.

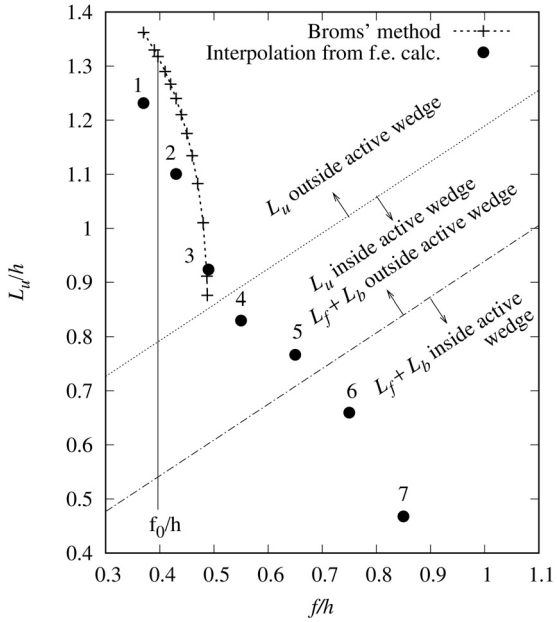

Figure 14 - Limit values of L_u/h obtained by interpolating results determined numerically (as represented in Fig. 13), as a function of f/h, for ϕ' = 24°, α = 15°, a/h = 0.2 and δ/ϕ' = 2/3.

sented in the same way as in Fig. 6. Taking as an example the value of ϕ' = 24°, a vertical line in Fig. 11 can be drawn and the points on that line or close to it can be used, either directly or by interpolating between two close values of the friction angle in such graphic. As can be seen from Fig. 11, few points would be provided in this way and so some more calculations were needed, using different values of f/h and different values of L_u/h and finding collapse values of the friction angle close to 24°. The values of L_u/h were determined by interpolating between those below that value and above it, for the same f/h ratio. The points used are represented in Fig. 13, linked by a solid line. This procedure is, of course, fastidious and can not be done systematically for different friction angles. But the case for ϕ' = 24° could be obtained that way and the results are represented in Fig. 14.

Figure 14 also shows the results obtained from Broms' method for the same friction angle, which allows comparison with the numerical results for the range of f/h for which Broms' method has solution. It can be seen that the significant decrease of the needed anchor length for small increases of the embedded length that had been observed previously is also present in the numerical calculations. In fact, points 1, 2 and 3 show this behavior, and the values of L_u/h obtained from the numerical calculations are quite similar to the ones obtained from Broms' method. For greater values of f/h, as seen before, Broms' method gives no solution (L_u is no longer outside the active wedge) and, as seen, this was part of the reasons for performing the numerical calculations. Numerical results were obtained and continue to show a decrease of the needed anchor length with increasing embedded length. This, however, happens with a significant change in the rate of the increase, with two different zones. In fact, points 4 and 5 show a much lower decrease of L_u/h with the increase of f/h; this rate seems to increase after point 5, with points 6 and 7.

The reason for this change seems to be related to the location of the bond length relatively to the active wedge. In fact, it was previously seen that Broms' method had a solution as long as the anchor length L_u was outside the active wedge. There are, therefore, no points obtained from this method below the line that represents the combination of f/h and L_u/h where L_u is at the failure surface of the active wedge. In the numerical calculations, however, the bond length to the right of L_u will also play some role in the equilibrium. And so it can be seen that this change in the rate of decreasing L_u/h with f/h happens almost exactly when the full anchor length ($L_f + L_b$, *i.e.*, $L_u + L_b/2$) is inside the active wedge.

For f/h ratios greater than around 0.85, results from the numerical calculations give collapse values of ϕ' less than 24°. This is expected, as f/h = 1.18 is the needed embedded length ratio for a cantilever wall for ϕ' = 24°, using, again, Frank *et al.* (2004) method and a coefficient of 1.2 for the embedded length, which means that for such value of f/h the anchor is no longer needed, the f.e.m. leading to a lower value.

It should also be mentioned that all numerical calculations used to obtain Fig. 14 were performed using a total excavation depth of 10 m and a bond length L_b = 5 m. This means that, for some of the lower values of L_u/h ratio adopted in the calculations used for the interpolations, some very small values of L_f had to be used. These values would not be used in practice, although they make sense in

Point in Fig. 14	f/h	L_u/h	"Left" mechanism ($\phi' < 24^o$)	"Right" mechanism ($\phi' > 24^o$)	Broms' mechanism
1	0.37	1.2315	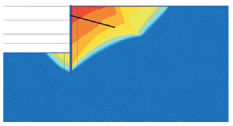 $L_u/h = 1.25$; $\phi' = 23.85^o$	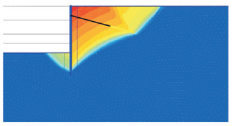 $L_u/h = 1.15$; $\phi' = 24.66^o$	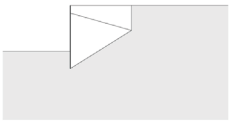 $L_u/h = 1.362$; $\phi' = 24^o$
2	0.43	1.1003	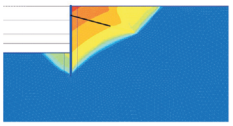 $L_u/h = 1.15$; $\phi' = 23.80^o$	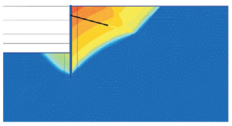 $L_u/h = 1.10$; $\phi' = 24.14^o$	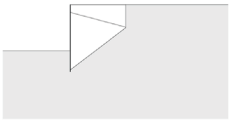 $L_u/h = 1.241$; $\phi' = 24^o$
3	0.49	0.9238	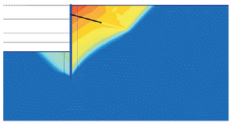 $L_u/h = 0.95$; $\phi' = 23.90^o$	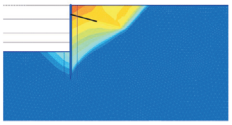 $L_u/h = 0.85$; $\phi' = 24.27^o$	—
4	0.55	0.8298	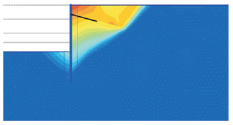 $L_u/h = 0.85$; $\phi' = 23.75^o$	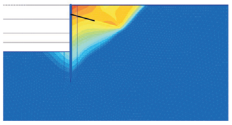 $L_u/h = 0.8$; $\phi' = 24.31^o$	—
5	0.65	0.7665	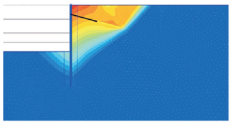 $L_u/h = 0.85$; $\phi' = 23.23^o$	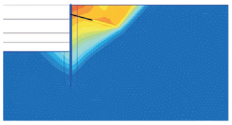 $L_u/h = 0.75$; $\phi' = 24.15^o$	—
6	0.75	0.6596	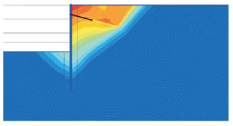 $L_u/h = 0.75$; $\phi' = 23.35^o$	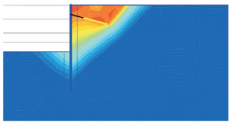 $L_u/h = 0.55$; $\phi' = 24.78^o$	—
7	0.85	0.4678	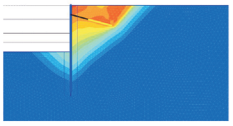 $L_u/h = 0.65$; $\phi' = 22.88^o$	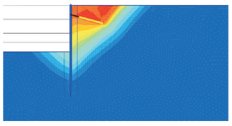 $L_u/h = 0.45$; $\phi' = 24.11^o$	—

Figure 15 - Mechanisms obtained for results presented in Fig. 14 (and results presented in Fig. 13 for interpolation for $\phi' = 24°$.

the perspective of the ratios L_u/h if greater values of h were used.

The mechanisms corresponding to the numerical results presented in Fig. 14 are represented in Fig. 15. As the points from Fig. 14 result from interpolation between two numerical calculations, the mechanisms included in Fig. 15 are shown for the two calculations, one on the "left" ($\phi' < 24°$) and the other on the "right" ($\phi' > 24°$). It can be seen that for the same f/h the two mechanisms are quite similar. It can also be observed that as f/h increases the mechanism becomes less typical of the overall stability and more triangular and rotational. The transition between the typical overall stability mechanisms and the triangular seems to correspond to cases 5 and 6.

The main result from these analyses seems to be that a decrease in the needed anchor length with increasing embedded length can indeed be obtained outside the range of validity of Broms' method. However, although possible from a limit state point of view, such solutions can only be practical if reasonable results are also obtained in a serviceability perspective. Such perspective needs to be verified by the designer for each particular case, but nevertheless the solutions for the case studied above can be a guide, if not for specific cases, at least as a way of evaluating if the study of such solutions can make sense.

To do so, results of the displacements obtained for each solution (the result that lead to the collapse friction angle closest to 24° was used) are represented in Fig. 16. Each solution is identified by a different line in this figure and the

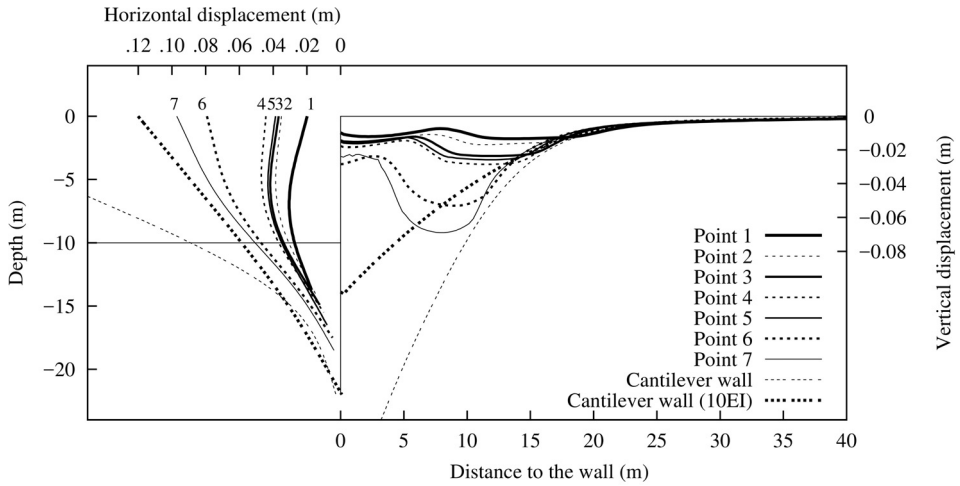

Figure 16 - Settlements and horizontal displacements of the wall for all construction stages for the cases of the points in Fig. 14.

horizontal displacements are also identified by the number corresponding to the points in Fig. 14. Analysis of this figure shows that: (1) the smallest displacements are obtained for case 1, for which no reduction in L_u was performed in exchange for an increase in f; (2) in general, displacements are greater for greater f_0 (and shorter L_u); (3) this trend is not exact for cases 4 and 5; displacements obtained for case 4 are slightly greater than the ones for case 3; (4) cases 2 to 5 show quite similar displacements; they correspond to cases where the bond length is interfering with the active wedges; (5) displacements for cases 6 and 7 are considerably greater than the displacements obtained for the other cases, with maximum horizontal displacements that seem unreasonable, as well as the settlements of the supported soil.

This last remark needs, however, some additional comment. In fact, the stiffness of the wall was kept constant in all calculations, which was considered suitable for comparison purposes. It should be noticed, however, that longer embedded lengths and shorter anchor lengths make the wall closer in its behavior to a cantilever wall. And if a cantilever wall was used for the same situation (a 10 m excavation in the same soil conditions), displacements would indeed be extremely large, as is also represented in Fig. 16, assuming elastic behavior of the wall. A significant part of these displacements are due to the flexibility of the wall, which means that a cantilever wall solution for this situation would need a more rigid structure. This case is also represented in Fig. 16 (marked as 10*EI*, because ten times the flexural stiffness of the previous calculations was assumed) and it can be observed that the displacements are much lower. So, back to comment (5) in the previous paragraph, it seems reasonable, in face of a particular design situation, to study the possibility of combining an increase in f_0 (and the correspondent decrease in L_u) with an increase in the flexural stiffness of the wall, which would to some extent reduce the displacements.

6. Conclusions

The overall stability of single-anchored retaining walls is an important stability verification that can be performed, in most situations, using Broms' method, a classical limit equilibrium method. Its simplicity and versatility allow the analysis of different geometrical and mechanical configurations. One of the parameters involved is the embedded length. A series of analyses using Broms' method showed that a small increase in the embedded length could lead to a significant decrease in the anchor length, which could be useful for economical or technical reasons, in particular in an urban environment, where intalling long anchors may not be possible.

Limitations of Broms' method do not allow the effect to be analysed for significant increases of the embedded length. For long embedded lengths the approach is not possible and a series of finite element calculations was performed. The procedure involved in this approach does not allow a systematic analysis of the problem for a wide range of cases, but it was used for one situation, as a way to evaluate if the increase in the embedded length could indeed be used for reducing anchor length.

Results of those analyses showed that such approach is possible and effective from an overall stability point of view, at a cost of some increase in the displacements, which can most probably be reduced by the increase of the flexural stiffness of the wall.

References

Broms, B.B. (1968). Swedish tieback system for sheet pile walls. Proc. 3rd Budapest Conf. Soil Mech. Found. Eng, pp. 391-403.

Costet, J. & Sanglerat, G. (1975). Cours pratique de Mécanique des Sols, Tome 2. Dunod, Paris, 352 p. In French.

Coulomb, C.A. (1776). Essai sur une application des règles des maximis et minimis à quelques problèmes de sta-

tique relatifs à l'architecture. Mem. Acad. Roy., 7, 38 p. In French.

Elton, D.J. & Whitbeck, J.E. (1997). Tieback design and construction. Final Report to the Alabama Highway Research Center. Technical report. Auburn University, Auburn, 72 p.

EN 1997-1 (2004). Eurocode 7, Geotechnical Design, Part 1: General Rules. CEN, European Committee for Standardization, Brussels.

Frank, R.; Bauduin, C.; Driscoll, R.; Kavvadas, M.; Ovesen, N.K.; Orr, T. & Schuppener, B. (2004). Designer's Guide to EN 1997-1 - Eurocode 7: Geotechnical Design - General Rules. Thomas Telford, London, 216 p.

Guerra, N.M.C.; Santos Josefino, C. & Antão, A.N. (2016). Overall stability of anchored retaining structures: revisiting Broms' method. In Lisyuk, M., Ulitsky, V. & Choudhury, D. (eds). Proceedings of two Seminars of TC207 ISSMGE in 2015. Soil-structure Interaction and Retaining Walls. Edinburgh and Pune. TC207, ISSMGE, pp. 25-32.

Hanna, T.H. (1982). Foundations in tension - ground anchors. McGraw-Hill, New York, 570 p.

Jelinek, R. & Ostermayer, H. (1967). Zur Berechnung von Fangedammen und verankerten Stützwänden. Die Bautechnik, 44(6):167-171;203-207. In German.

Kérisel, J. & Absi, E. (1990). Active and Passive Earth Pressure Tables. 3rd ed. Balkema, Rotterdam, 220 p.

Kranz, E. (1953). Über die Verankerung von Spundwänder. Wilhelm Ernst & Sohn, Berlin, 53 p. In German.

Littlejohn, G.S. (1972). Anchored diaphragm walls in sand. Ground Engineering, 5(1):12-17.

Matos Fernandes, M. (1990). Earth Retaining Structures. FEUP, Porto. In Portuguese.

Müller-Breslau, H. (1906). Erddruck auf Stützmauern. Kroener, Stuttgart. In German.

Plaxis (2014). Plaxis 2D Manual. Brinkgreve *et al.* (eds). Delft.

Puller, M. (1996). Deep excavations. A practical manual. Thomas Telford, London, 448 p.

Ranke, A. & Ostermayer, H. (1968). Beitrag zur Stabilitätsuntersuchung mehrfach verankerter Baugrubenumschließungen. Die Bautechnik, 45(10):341-350. In German.

Santos Josefino, C.; Guerra, N.M.C. & Antão, A.N. (2014). Review of Kranz's and Brom's methods applied to single anchored walls: preliminary results. In Proceedings of the 14th National Geotechnical Conference, Covilhã, UBI, April 6-9. Published in CD. In Portuguese.

Schanz, T.; Vermeer, P. & Bonnier, P. (1999). The hardening-soil model: formulation and verification. In: Beyond 2000 in Computational Geotechnics. Balkema, Rotterdam, pp. 281-290.

Schnabel Foundation Company (1996). Draft final report - ground anchor walls: Research results and recommendations. Technical report, US Department of Transportation, Federal Highway Admnistration.